Mapana – Journal of Sciences
2023, Vol. 22, No. 1, 205-243
ISSN 0975-3303 | https://doi.org/10.12723/mjs.64.10

Theoretical and Experimental Investigations of Antibiotic Agents Sulfamethoxazole (SMX) and Trimethoprim (TMP) by Density Functional Theory

Annoji Reddy R [*†], Vibha[*], Prachalith N.C.[*], Ravikantha M.N.[‡*], Shilpa K.G.[§], Thipperudrappa J[*]

Abstract

In this manuscript, a complete theoretical and experimental investigation of antibiotic agents Sulfamethoxazole (SMX) and Trimethoprim (TMP) was performed at B3LYP, CAM-B3LYP, B3PW91/6-311++G (d,p) levels through DFT (density functional theory). The bond length and bond angles of SMX and TMP are calculated and compared with existence literature data. The global reactivity descriptors have been estimated from HOMO - LUMO energies to understand the stability and chemical reactivity of investigated molecules. The electrophilic sites present in the investigated molecules have been identified by using MEP. Mulliken atomic charge distribution has been analysed at three different levels of theories/basis set. The Non-linear optical

[*] Department of Physics, Vijayanagara Sri Krishnadevaraya University, Ballari- 583 104, India.
[†] Department of Physics, GVVP GFGC, Hagari Bommanahalli-583 212, India.
[‡] Department of Physics, Government Science College, Chitradurga-577 501, India.
[§] Department of Chemistry, Vijayanagara Sri Krishnadevaraya University, Ballari- 583 104, India.
Email: jtrphy2007@gmail.com

parameters have been calculated for investigated molecules to understand their suitability in non-linear optics. The NBO study has been utilised to disclose the strongest inter-molecular interactions. The vibrational assignment of SMX and TMP molecules has been performed with the assistance of DFT coupled with the VEDA program.

Keywords: Sulfamethoxazole, Trimethoprim, DFT, VEDA, FMO, NLO

1. Introduction

The drug molecules Sulfamethoxazole (SMX) and Trimethoprim (TMP) act as antimicrobial agents used in the treatment of bacterial infections, and collectively they are called co-trimoxazole. Co-trimoxazole is abbreviated as TMP-SMX. These drugs are cost-effective and used for many types of illnesses like bacterial infections and urinary tract infections. SMX is a well-known antibiotic drug and it is the derivative of Sulfonamide, used for the treatment of bacterial infections such as bronchitis, prostatitis and urinary tract infections[1]. SMX in combination with trimethoprim of the ratio 5:1 is used as Co-trimaxazole [2]. It is also used to cure toxoplasmosis. SMX contains Sulfonamide functional groups which might be responsible for the antimicrobial activities[3]. For the treatment of sinusitis, SMX can be used as an alternative to Amoxicillin. TMP is called an antifolate antibiotic often used in combination with SMX to treat many infections like respiratory tract, and gastrointestinal tract infections[4], [5].TMP is also used to treat certain types of pneumonia when it combines with other drugs.

In recent years, computational studies have become popular in different research areas because of their potentiality in predicting molecular properties. Specifically, the density functional theory (DFT) related works becoming more widespread due to its efficiency in understanding the complexity of chemical and biological mechanisms[6]. The computational studies related to SMX and TMP through DFT have their intensive contributions in theoretical research[7]–[13]. In literature, the detailed structural and vibrational assignment of SMX and TMP has been performed using single theory and single basis set. However, there is a lack of studies on the

theoretical investigation of SMX and TMP with different theories and basis sets. The investigations based on different theories and basis sets are essential to estimate exact properties of molecules.

In the present study, geometrical parameters of SMX and TMP drug molecules, and vibrational assignments with PED contribution are also carried out. Using different theories and a single basis set geometrical parameters, binding sites, electronic states, molecular electrostatic potential (MEP), chemical reactivity, optical properties (NLO), Mulliken atomic charge, NBO (Natural bonding orbitals) and FTIR spectra have been computed.

2. Materials and methods

2.1 Materials

Sulfamethoxazole (SMX) and Trimethoprim (TMP) with 99% purity were purchased from Sigma Aldrich, India. Chemical structure of SMX and TMP is given in Figure.1.

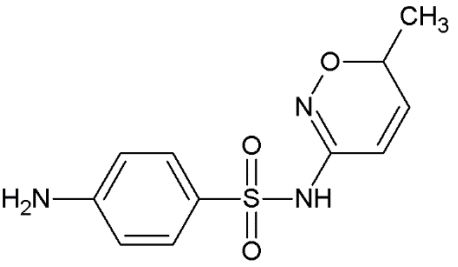

Fig.1(a)

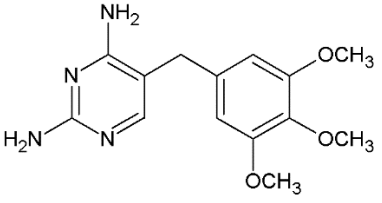

Fig.1(b)

Fig.1. Chemical structure of (a) SMX and (b)TMP

2.2 Experimental method

The FT-IR spectra of SMX and TMP were recorded using Perkin's-Spectrum 2 spectrometer in the spectroscopic range 4000-400 cm^{-1}, using the KBr pellet technique.

2.3 Computational method

The theoretical calculations of SMX and TMP has been carried out with the help of Gaussian-09 software using DFT method at B3LYP, CAM-B3LYP and B3PW91/6-311++G (d,p) level. [14][15]. The factors d and p present in the basis set are used to treat the heavy atoms containing polar bonds of sulfa and nitro groups[16]. The optimization was carried out in the gaseous phase and optimised geometry was used for further calculations. Vibrational Energy Distribution Analysis (VEDA) software is used for the detailed assignments of vibrational frequencies[17].NBO version 3.1 is used to compute the NBO properties[18].

3. Results and Discussion

3.1. Molecular Geometrical parameters

The molecular geometries of SMX and TMP were optimised at B3LYP, CAM-B3LYP and B3PW91/6-311++G(d,p) by DFT. The optimised geometries with dipole moment vector of SMX and TMP obtained at B3LYP theory are given in Figure.2. The summary obtained for optimized structure of SMX and TMP shows that both the molecules belong to the C_1 point group. The dipole moment values 4.16D (B3LYP), 5.02D (CAM-B3LYP)and 4.76D (B3PW91) are obtained for ground state of SMX. The dipole moment values 1.27D (B3LYP), 1.21D (CAM-B3LYP) and 1.26D (B3PW91) are obtained for ground state of TMP. This indicates that SMX is more polar in ground state than TMP. Using optimized molecular geometries, the bond length in angstroms Å, are tabulated in Table 1 (a) &1(b) and bond angles in degree (^{o}) are tabulated in Table 2(a) & 2(b). For SMX and TMP calculated at different levels of theory with 6-311G(d,p) basis set. The experimental values of bond length and bond angle for SMX are also given in Table 1(a) and Table 2(a) respectively[19]. However, in the literature no reports were found on experimental values of bond lengths and bond angles for TMP. From Table 1(a) it is clear that in case of SMX, the bond lengths estimated from three

different methods are nearly same (varies by less than 1%) and are slightly deviated from experimental data (less than 5%). This slight deviation could be due to the reason that experimental values are determined in the solid phase and computation is carried out in the gaseous phase. The bond angles between the inter atomic bonds in SMX obtained by the three levels are also nearly same and are slightly deviated from experimental data. Similarly, for TMP the values of bond lengths and bond angles computed from three different methods are nearly same.

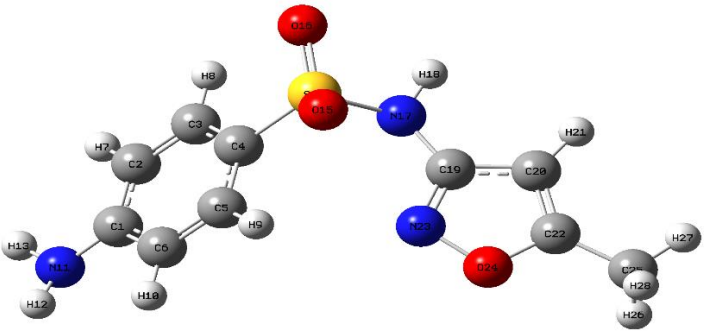

Fig.2(a)

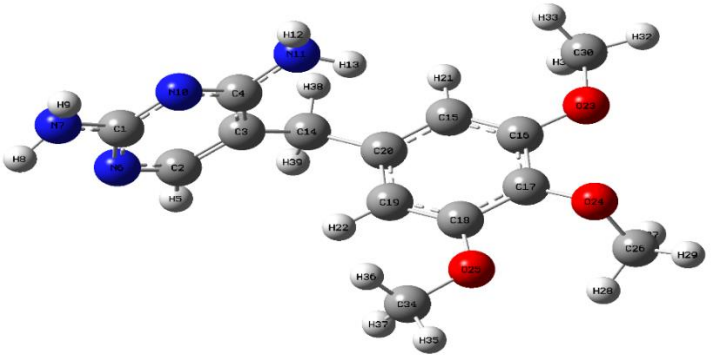

Fig.2(b)

Fig.2 Optimized Geometrical Structure of (a) SMX and (b) TMP

Table 1(b). Selected Bond lengths of TMP compound

Bond length (Å)	**B3LYP**	**CAM-B3LYP**	**B3PW91**
C1-N6	1.340	1.333	1.338
C1-N7	1.369	1.362	1.365
C1-N10	1.340	1.335	1.337
C2-C3	1.385	1.377	1.383
C3-C4	1.418	1.413	1.416
C2-N6	1.337	1.332	1.334
C4-N10	1.335	1.328	1.332
C4-N11	1.370	1.364	1.365
N7-H8	1.006	1.005	1.005
N7-H9	1.006	1.004	1.005
N11-H12	1.009	1.008	1.008
N11-H13	1.009	1.008	1.009
C16-O23	1.361	1.354	1.355
C17-C18	1.405	1.398	1.403
C17-O24	1.368	1.362	1.362
C18-O25	1.361	1.354	1.355
C19-C20	1.396	1.389	1.393
O23-C30	1.420	1.413	1.413
O24-C26	1.43	1.421	1.423

Table 2(a). Selected Bond angles of SMX compound

Bond Angle (^{0})	**Experimental**	**B3LYP**	**CAM-B3LLYP**	**B3PW91**
C2-1C-C6	117.5	118.8	119.0	118.8
C2-C1-N11	122.6	120.5	120.4	120.5
C6-C1-N11	119.9	120.5	120.5	120.5

Bond Angle (^{0})	Experimental	B3LYP	CAM-B3LLYP	B3PW91
C1-C2-C3	122.3	120.5	120.4	120.5
C2-C3-C4	120.0	119.5	119.5	119.5
C3-C4-C5	118.8	120.8	120.8	120.8
C3-C4-S14	121.1	119.2	119.2	119.3
C5-C4-S14	120.0	119.8	119.8	119.7
C4-C5-C6	120.0	119.3	119.3	119.4
C1-C6-C5	120.7	120.7	120.6	120.7
C4-S14-O15	110.4	108.8	108.7	108.7
C4-S14-O16	108.0	109.1	108.9	109.1
C4-S14-N17	107.4	104.8	105.3	104.8
O15-S14-N16	119.8	121.6	121.6	121.6
O15-S14-N17	103.6	109.4	109.1	109.4
O16-S14-N17	106.8	101.5	101.7	101.5
S14-N17-C19	122.4	124.4	125.2	124.6
N17-C19-C20	129.3	125.9	125.9	126.1
N17-C19-C23	119.6	121.7	121.9	121.7
C20-C19-N23	111.6	112.1	112.0	112.0
C20-C22-O24	110.3	109.6	109.6	109.5
C20-C22-C25	133.7	133.4	133.5	133.4
O24-C22-C25	115.9	116.8	116.7	116.9
C19-N23-O24	105.4	104.8	105.1	105.0
C22-O24-N23	108.0	109.6	109.6	109.8

3.2. Frontier molecular orbitals (FMO)

HOMO-LUMO are jointly termed as FMO (Frontier Molecular orbitals). HOMO-LUMO act as electron donor and acceptors respectively, which gives more information about the chemical

stability and chemical reactivity of the molecules. HOMO-LUMO for SMX and TMP were computed at B3LYP, CAM-B3LYP and B3PW91/ 6-311++G(d,p) levels. These values of HOMO and LUMO energies are given in Table 2 along with energy gaps for all the theories. The HOMO and LUMO energies obtained from B3LYP and B3PW91 are nearly same. However, these values are over estimated in case of CAM-B3LYP. This could be due to the reason that CAM-B3LYP method considers long range corrections, whereas the B3LYP and B3PW91 functions considers short range corrections[20].Figure.3. shows the electron density distribution over the HOMO and LUMO energy levels and energy gaps between them for SMX and TMP obtained from B3LYP theory. HOMO level of SMX exhibits electron density distribution over the entire benzene-sulfonamide group. Also electron density distribution is extended over nitrogen and oxygen atoms in isoxazole group. In LUMO, the electron density distribution over the nitrogen and oxygen atoms is observed to be shifted to benzene sulfonamide moity. This infers the possible charge transfer takes place within the molecule. The HOMO level of TMP indicates that electron distribution is spread over the entire molecule excluding on methoxy groups attached to benzene ring. In LUMO of TMP it has been observed that electron density has slightly increased over the pyrimidine ring. This again indicates the possible intramolecular charge transfer.

By using HOMO-LUMO values for a molecule, the reactivity descriptors namely ionization potential (IP),electronegativity (χ), electron affinity (EA), electrophilicity index (ω), hardness (η), and softness (S) values were computationally determined for three levels of theory with 6-311++G(d, p) basis set and are also tabulated in Table.3. The ionization potential gives an idea about electron donating capacity of the system, lower the IP value, better will be the electron donating capacity. TMP having the lower value of IP exhibits better electron donating capacity than that of SMX. Higher values of electronegativity and electron affinity indicates more electron accepting ability. SMX having more electronegativity and electron affinity value in three levels of theory than TMP indicates SMX is having better electron accepting ability than TMP. Electrophilicity index is another important global reactive descriptor that talks about electron-accepting ability. The greater value of

electrophilicity index signifies better electron-accepting capacity. From the above-studies SMX is having more electrophilicity index as compared to TMP indicating that it has more electron accepting ability. The compound with a high energy gap is harder and less reactive or vice-versa. As observed in the studied molecules, SMX is harder and less reactive as compared to TMP which is softer and more reactive [21]–[24].

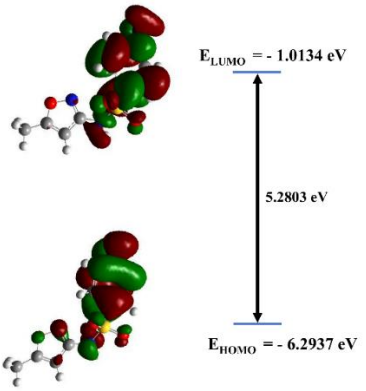

Fig 3(a)

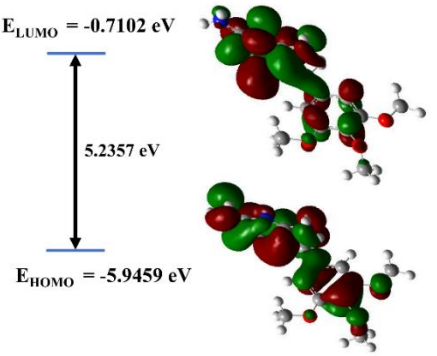

Fig 3(b)

Fig.3. HOMO-LUMO orbitals of (a) HOMO-LUMO energy of (a) SMX and (b) TMP molecules

Table 3. Reactivity descriptors of SMX and TMP molecules

Parameters	SMX			TMP		
	B3LYP	CAM-B3LYP	B3PW91	B3LYP	CAM-B3LYP	B3PW91
E_{HOMO} (eV)	-6.2937	-7.6572	-6.2964	-5.9459	-7.3440	-5.9530
E_{LUMO} (eV)	-1.0134	0.1251	-0.9774	-0.7102	0.2345	-0.6571
ΔEgap (eV)	5.2803	7.5321	5.319	5.2357	7.1090	5.2900
Ionization Potential(IP)	1.0134	-0.1251	0.9774	0.7102	-0.2345	0.6571
Electronegativity (χ)	4.1602	3.7034	4.1256	3.6831	3.4374	3.6336
Electron Affinity (EA)	6.2937	7.6572	6.2964	5.9459	7.3440	5.9530
Electrophilicity (ω)	2.5279	1.8224	2.4868	2.1154	1.6673	2.0626
Hardness (η)	2.6401	3.8912	2.6595	2.6178	3.7893	2.6479
Softness (s)	0.3787	0.2569	0.3760	0.3819	0.2638	0.3776

3.3. Molecular Electrostatic Potential (MEP)

MEP is used as an invaluable tool for the qualitative interpretation of the electrophilic and nucleophilic reactions for the study of hydrogen bonding interactions. In the MEPs, red colour is indicated as the maximum negative region, which is the preferred site for an electrophilic attack, yellow colour indicates the slightly electron rich region, light-blue colour indicates the slightly electron deficient region, green colour indicates the neutral region and blue colour indicates the maximum positive region, which is the preferred site for nucleophilic attack. MEP also displays , positive, negative, and neutral electrostatic potential regions[25], [26].The MEP mapped surface for SMX and TMP obtained from three theories are shown in Figure.4. The MEP maps computed by different levels are nearly identical. In case of SMX, the maximum electron density is concentrated near - O (oxygen) atoms which are bonded to-S

(sulphur) and hence these sites are preferred sites for an electrophilic attack. The minimum electron density is concentrated near the nitrogen atom of benzene sulfonamide group and therefore this site is a favoured location for an attack of nucleophile. In case of TMP, the maximum electron density is concentrated near the oxygen atoms bonded to benzene ring and therefore these sites are favoured location for an attack of electrophile. The minimum electron density is concentrated near the amine groups of pyrimidine and hence these are preferred sites for nucleophilic attack. These results indicate that the investigated molecules possesses both attacking sites (electrophilic and nucleophilic) and hence they are chemically reactive.

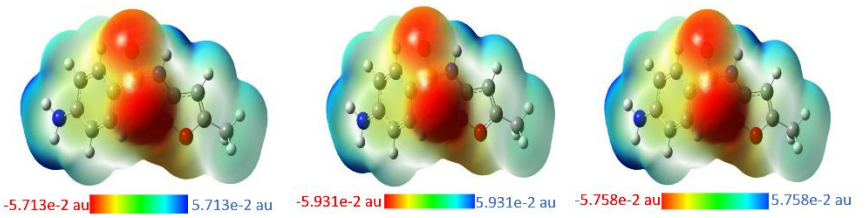

Fig.4a

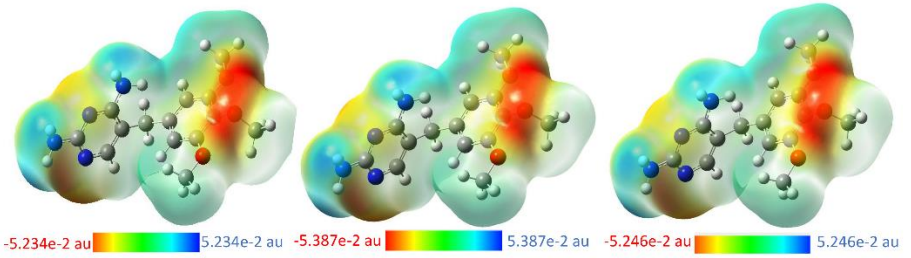

Fig.4b

Fig.4. Molecular Electrostatic Potential maps of (a) SMX and (b) TMP molecules

3.4. Mulliken atomic charge

Mulliken charge analysis is a helpful tool used to study the atomic charge distribution and also the dependence of electronic structure, dipole moment, and polarizability of the molecules based on the distribution of atomic charge. The Mulliken atomic charge distribution for optimized molecules is obtained at different levels of theory and no appreciable variation is noticed. The charge distribution graph of SMX and TMP plotted for B3LYP level are represented in Figure.5. In SMX, carbon atoms C3 and C20 shows positive charge and all other carbon atoms shows the negative charge. The N11, N17, N23, atoms show the negative charge. The O15, O16 atoms shows the negative charge whereas the O24 atom shows positive charge. S14 attached to the O15 and O16 shows the positive charge. In TMP, all the carbon atoms except C3, C19, and C20 shows negative charge. C14 shows the more negative charge compared to all other carbon atoms due to the attachment of heavier functional groups. N6, N7, N10, N11, and O23, O24, O25 atoms are showing negative charge. The variation in the charge distribution across different atoms is due to the intramolecular charge transfer among the various types of inter atomic bonds.

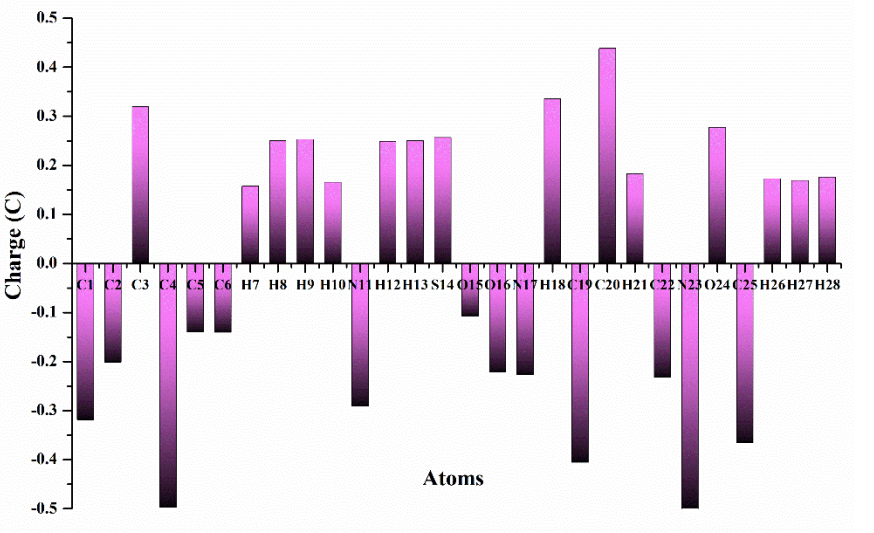

Fig.5 (a)

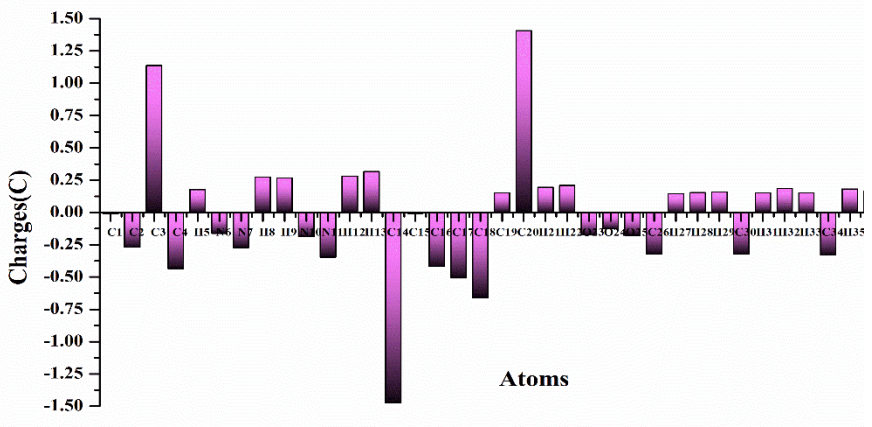

Fig.5 (b)

Fig.5. Mulliken Plot for (a) SMX and (b) TMP molecules.

3.5 Non-linear Optical Properties (NLO)

Organic molecules have their importance in several biochemical and sensing applications due to their unique dipole moment (μ), polarizability (α) and hyperpolarizability (β) values which are collectively called Non-linear optical properties. These molecules exhibit NLO property by the interaction of the electrons in the molecule with the electric field of the light radiation. The NLO properties of the molecule are also depending on the overall geometry of the molecule. The SMX and TMP are geometrically optimized using B3LYP, CAM-B3LYPand B3PW91/6311-G++(d, p) level through the DFT approach. The obtained values of NLO parameters from three different theories are nearly same in magnitudes and data obtained for B3LYP level is given in Table 4. The NLO property of molecules can be well estimated by the comparative observations of the obtained hyperpolarizability values with the hyperpolarizability value of Urea which is a prototypic molecule concerned with the NLO property. Urea has a hyperpolarizability value of about 0.343×10^{-30} e.s.u [27].The hyperpolarizability value (β_o) for the SMX and TMP are found to be 1.74×10^{-30} e.s.u and 4.71×10^{-30} e.s.u respectively. As the β values obtained through the computational technique for SMX and TMP are greater than that of the β value of Urea, both SMX and TMP can be used for better NLO applications.

Table 4. Non-linear Optical Properties of SMX and TMP molecules

Parameters	**SMX**	**TMP**
β_{xxx}	41.890	-100.184
β_{xxy}	-182.948	-57.559
β_{xyy}	-182.117	142.833
β_{yyy}	13.420	218.652
β_{xxz}	41.766	-278.343
β_{xyz}	0.342	135.313
β_{yyz}	-16.784	-120.128
β_{xzz}	22.465	89.226
β_{yzz}	52.777	36.084
β_{zzz}	88.968	-92.525
β_o (e.s.u) $x10^{-30}$	1.74	4.71
μ_x	1.851	0.454
μ_y	-2.300	-0.018
μ_z	-1.155	0.213
μ(D)	3.170	0.502
α_{xx}	232.150	280.894
α_{xy}	5.051	-24.767
α_{yy}	187.456	208.943
α_{xz}	4.687	-5.100
α_{yz}	-9.733	3.017
α_{zz}	111.986	165.377
α_{tot} (e.s.u) $x10^{-24}$	177.1973	218.4047

3.6. Natural Bonding Orbitals (NBO)

Natural bond orbitals lie between the atomic orbitals and the molecular orbits which represents the maximum probability of the distribution of electrons in the molecular system[28]. Bonding orbitals in the molecule are considered as Lewis's orbitals with the maximum occupancy of two electrons and antibonding orbitals are considered as the non-Lewis orbitals with a parameter of electron occupancy nearly equal to zero. Second order Fock-Matrix method has been used to estimate the stabilized energy E(2) of the molecule based on the interaction between the bonding (donors) and antibonding orbitals (acceptor). [29]

More stabilization energy leads to the more intensive interactions of donors and acceptors and the complex structure conjugation. NBO iterations for the SMX and TMP structures are carried out through the DFT approach using Gaussian 09 software at B3LYP, CAM-B3LYP, andB3PW91/6311-G++(d, p) levels. Table 5(a) and 5(b) shows values of NBO parameters of SMX and TMP molecules computed at B3LYP level of theory. NBO data obtained for the SMX shows that the intermolecular interaction between LP(2) O24 and π*C20-C22 has more stabilization energy of36.22 kcal/mol compared to all-other interactions. In TMP, the interaction between σC14-H39and σ C34-H37 has more stabilization energy of 51.47 kcal/mol compared to other interactions. Both these interactions in the SMX and TMP are observed as highly intensive interactions as evidenced from the highest value of Fock-matrix element F_{ij}.

Table 5(a). NBO analysis of SMX molecule.

Donors(i)	Occupancy	Bond Type	Acceptors (j)	Occupancy	Bond Type	E(2)kcal/mol	E_j-E_i(a.u.)	F_{ij}(a.u.)
O24	1.726	LP(2)	C20-C22	0.266	π*	36.22	0.35	0.101
N11	1.820	LP(1)	C1-C6	0.402	π*	31.27	0.32	0.094
C1-C6	1.605	π	C4-C5	0.416	π*	29.94	0.27	0.081
N17	1.830	LP(1)	C19-N23	0.368	π*	29.65	0.32	0.091
C20-C22	1.826	π	C19-N23	0.368	π*	27.06	0.29	0.083
C4-C5	1.688	π	C2-C3	0.308	π*	25.13	0.29	0.076
C2-C3	1.709	π	C1-C6	0.402	π*	23.07	0.28	0.074

Donors(i)	Occupancy	Bond Type	Acceptors (j)	Occupancy	Bond Type	E(2)kcal/mol	E_j-E_i(a.u.)	F_{ij}(a.u.)
O15	1.716	LP(3)	S14-N17	0.286	σ*	21.42	0.38	0.081
O16	1.795	LP(3)	S14-O15	0.147	σ*	17.93	0.58	0.093
O15	1.814	LP(2)	C4-S14	0.179	σ*	16.40	0.46	0.078
O15	1.761	LP(3)	S14-O16	0.138	σ*	15.78	0.57	0.087
O16	1.820	LP(2)	C4-S14	0.179	σ*	15.52	0.47	0.076
C1-C6	1.605	π	C2-C3	0.308	π*	14.67	0.28	0.059
C2-C3	1.709	π	C4-C5	0.416	π*	14.26	0.28	0.058
O16	1.795	LP(3)	S14-N17	0.286	σ*	13.76	0.38	0.066
O24	1.726	LP(2)	C19-N23	0.368	π*	13.59	0.34	0.062
C4-C5	1.688	π	C1-C6	0.402	π*	13.51	0.29	0.057
C19-C20	1.964	π	C22-C25	0.016	σ*	7.410	1.10	0.081
C19-N23	1.928	π	C20-C22	0.266	π*	7.280	0.35	0.047

Table 5(b). NBO analysis of TMP molecule.

Donors(i)	Occupancy	Bond Type	Acceptors (j)	Occupancy	Bond Type	E(2)kcal/mol	E_j-E_i(a.u.)	F_{ij}(a.u.)
C14-H39	1.967	σ	C34-H37	0.018	σ	51.47	5.55	0.479
N7	1.792	LP(1)	C1-N6	0.461	π*	43.89	0.28	0.106
N11	1.785	LP(1)	C4-N10	0.449	π*	41.16	0.29	0.104
C4-N10	1.743	π	C1-N6	0.461	π*	37.42	0.31	0.101
C1-N6	1.707	π	C2-C3	0.311	π*	33.58	0.33	0.094
C2-C3	1.716	π	C4-N10	0.449	π*	31.94	0.26	0.085
O25	1.840	LP(2)	C18-C19	0.416	π*	29.91	0.34	0.097
C3-C14	1.971	σ	C34-H37	0.018	σ *	29.63	5.69	0.367
C14-C20	1.972	σ	C34-H37	0.018	σ *	28.99	5.68	0.363
O23	1.840	LP(2)	C16-C17	0.411	π*	28.26	0.34	0.093
C18-C19	1.671	π	C15-C20	0.407	π*	24.79	0.29	0.077

Donors(i)	Occupancy	Bond Type	Acceptors (j)	Occupancy	Bond Type	E(2)kcal/mol	E_j-E_i(a.u.)	F_{ij}(a.u.)
C16-C17	1.653	π	C18-C 19	0.416	π*	23.70	0.29	0.075
C15-C20	1.719	π	C16-C17	0.411	π*	23.11	0.28	0.074
C16-C17	1.653	π	C15-C20	0.407	π*	16.63	0.29	0.063
C18-C19	1.671	π	C16-C17	0.411	π*	15.88	0.28	0.061
C15-C20	1.719	π	C18-C19	0.416	π*	14.24	0.28	0.059
C14-H38	1.971	σ	C34-H37	0.018	σ	12.89	5.56	0.239
N6	1.910	LP(1)	C1-N10	0.037	σ	12.21	0.87	0.093
N10	1.900	LP(1)	C1-N6	0.038	σ	11.44	0.87	0.09

3.7. FTIR Analysis

Vibrational spectroscopy is a prototypical tool used to determine the functional groups of the molecule. The experimental FT-IR spectra were recorded (4000 $cm^{-1}$to 400cm^{-1}) in the solid phase and theoretical IR were obtained from the DFT approach at different levels of theory in gaseous phase. The theoretical and experimental infrared spectra are represented in Figure 6. The small variations have been observed in experimental spectral peaks compared to theoretical peaks obtained for three levels of theory. One of the reasons for these variations is due to the fact that computed spectra are based on gaseous state of the sample, whereas experimental spectra are based on solid state of the sample. The other reason is attributed to the an harmonicity of vibrations in experimental spectra. In both the molecules, the vibrations obtained by B3LYP method better matches with experimental vibrations. Theoretical and experimental frequencies with potential energy distributions (% PED) are presented in Table 6. The tabulated wavenumbers shows the various modes of vibrations namely stretching mode, bending mode and also torsional mode occur in the molecules SMX and TMP. The assignment of vibrations for observed wavenumbers based on PED is carried out in the following sections.

Vibrations in SMX

N-HVibrations:

The N-H group vibrations present in hetero-aromatic compounds are expected in the range of 3500 to 3220 cm^{-1}[30], [31]. In SMX, the theoretical N-H frequencies are at 3586(forB3LYP), 3620(for CAM-B3LYP) and 3608 (for B3PW91) cm^{-1} with 50% PED and the corresponding experimental frequency is observed at 3468 cm^{-1}. This indicates that B3LYP method better approximates experimental value.

NH_2 Vibrations:

The NH_2produces scissoring mode of vibration in the frequency range of 1700-1600 cm^{-1}[32]–[34]. In SMX, the theoretical frequencies at 1663 (for B3LYP), 1696 (for CAM-B3LYP) and 1668 (for B3PW91) cm^{-1} with 75% PED are designated as scissoring -NH_2 mode of vibrations. The experimental scissoring mode of vibrations are observed at 1710 cm^{-1}.

SO_2Vibrations:

The SO_2 scissoring mode of vibrations are expected in the frequency range 600-520

cm^{-1}[35]. In SMX, computed frequencies at 561 (for B3LYP), 576 (for CAM-B3LYP) and 565(for B3PW91) cm^{-1} with PED of -23% are assigned to SO_2 scissoring mode. The experimental vibrations are observed at 580 cm^{-1}. The SO_2 out of plane bending are expected in the frequency range of 555 – 445 cm^{-1}[23]. The theoretically obtained bands at 508 (for B3LYP), 515(for CAM-B3LYP) and 509(for B3PW91) cm^{-1} with 22% of PED corresponds to SO_2 out of plane bending vibrations.

S-N Vibrations:

The S-N stretching mode is expected in the range 935 – 875 cm^{-1}[36]. For SMX molecule, computed bands appeared at 818 (for B3LYP), 848 (for CAM-B3LYP) and 830 (for B3PW91) $cm^{-1}$are designated as S-N asymmetric stretching mode of vibrations with-23% PED. However, no experimental peaks were observed for these mode of vibrations.

C=N and C-N Vibrations:

The C=N produces stretching mode of vibrations within the range 1550-1700 cm^{-1}[25].

For SMX molecule, theoretically obtained bands at 1537 (for B3LYP), 1587 (for CAM-B3LYP) and 1556 (for B3PW91) $cm^{-1}$are designated to N23=C19and N17 - C19 mode of vibrations with 51% and -11%PED respectively. The N23- C19 are correspond to symmetric stretching mode, whereas N17 - C19vibrations correspond to asymmetric stretching mode. These frequencies are experimentally observed at 1575 cm^{-1}.

C-N produces stretching mode of vibrations within the range 1330-1220 cm^{-1}. For SMX, computed wavenumbers appeared within the range of 1318-1160 (for B3LYP) , 1339-1177 (for CAM-B3LYP) and 1329-1164 (for B3PW91)and are designated to C-N stretching mode of vibrations. These frequencies are appeared experimentally within the range of 1311-1187 cm^{-1}

C-H Vibrations:

The C-H produces stretching vibrations in the frequency range of 3180-3000 cm^{-1}[37]. Many such vibrations are observed in the computed spectra. The computed wavenumbers within the range of 3260 –3038 (for B3LYP) ,3283 –3067 (for CAM-B3LYP) and 3273 –3049 (for B3PW91) $cm^{-1}$are assigned to C-H vibrations in the benzene and methyl isoxazole groups. The vibrations are observed experimentally in the range 3245 – 2933 cm^{-1}.

Vibrations in TMP

NH_2 Vibrations:

The NH_2 group attached to the pyridine ring shows the stretching, scissoring and rocking modes of vibration around 3500-3000, 1700-1600 and 1150-099 cm^{-1} respectively [38] . The TMP contain two NH_2 groups namely NH_2(β1)and NH_2(β2). NH_2(β1) group shows scissoring mode of vibration at 1653 (for B3LYP), 1688 (for CAM-B3LYP) and 1664 (for B3PW91) cm^{-1}obtained with PED contribution 53% and experimental peak were observed at 1655cm^{-1}. The NH_2(β2) group also shows scissoring mode of vibration at 1640 (for B3LYP), 1668 (for CAM-B3LYP) 1649 (for B3PW91) cm^{-1} with PED contribution 21% and experimental peak were observed at 1643cm^{-1}.

C=N, C-N Vibrations:

The C=N produces stretching vibrational modes within the range 1700-1550cm^{-1}. In TMP the theoretically obtained wavenumbers are 1590 (for B3LYP), 1629 (for CAM-B3LYP) and 1607(for B3PW91) cm^{-1} with 39%PED and they corresponds to C=N stretching vibrational modes. However, the corresponding experimental frequencies are not appeared.

The C-N stretching modes are generally appeared in the range 1330-1220 cm^{-1}. In TMP, theoretical wavenumbers correspond to C4-N11appeared at 1340 (for B3LYP), 1351(for CAM-B3LYP) and 1341(for B3PW91) cm^{-1}with 10% PED contribution and are designated to C-N stretching mode of vibrations. These frequencies are experimentally appeared at 1335 cm^{-1} . Also, the frequencies appeared within the range 1303-1309 (for B3LYP), 1306-1317(for CAM-B3LYP) and 1311-1328 (for B3PW91) cm^{-1}are designated to stretching ode of C2-N6. The corresponding experimental frequencies are not appeared.

O-CH_3 Vibrations:

In the O-CH_3 group, the C-H symmetric and asymmetric stretching vibrations are expected within the range of 2900-2800 and 3100-2900 cm^{-1} respectively. In TMP, computed wavenumbers at 3004, 3031 and 3010 cm^{-1}respectively fromB3LYP, CAM-B3LYP and B3PW91 theories with PED contribution of 91% are assigned to C30-H31 symmetric stretching vibration. These vibrations are observed experimentally at 2964 cm^{-1}. The computed wavenumbers at 3068, 3099 and 3082 cm^{-1}respectively from B3LYP, CAM-B3LYP and B3PW91 theories corresponding to C34-H36 vibration with PED contribution -99% are assigned to asymmetric stretching vibration and is experimentally observed at 3014 cm^{-1}. The computed wavenumbers at 3123, 3151 and 3132 cm^{-1}corresponding to C26-H27 vibration respectively from B3LYP, CAM-B3LYP and B3PW91 theories with PED contribution of -13% are also assigned to asymmetric C-H mode of vibration. However, these vibrations are not observed experimentally.

In TMP, the computed wavenumbers at 1160, 1177 and 1163 cm^{-1} corresponding to C30 -O23 vibrations with 64% PED contribution from B3LYP, CAM-B3LYP and B3PW91 respectively are assigned to

C-O stretching mode of vibration. These vibrations are observed at 1130 cm^{-1}in experimental spectrum. The wavenumbers computed at 1027, 1061 and 1049 cm^{-1}corresponding to C26-O24 with 77% PED contribution from B3LYP, CAM-B3LYP and B3PW91 respectively are also assigned to C-O stretching mode of vibrations. These vibrations are observed at 1000 cm^{-1}experimentally. These wavenumbers are in good agreement with literature values[39].

In the O-CH3 bond group, the C-H symmetric and asymmetric vibrations are expected respectively within the range of 2000-2800 and 3100-2900 cm-1. In TMP, theoretically obtained wavenumbers 3004 (for B3LYP), 3031(for CAM-B3LYP) and 3010 (for B3PW91) with 91% PED are designated to C30-H31 symmetric stretching vibrations. The respective experimental frequency is appeared at 2964 cm^{-1}. The theoretically obtained frequencies 3068 (for B3LYP), 3099 (for CAM-B3LYP) and 3082 (for B3PW91) cm^{-1} corresponds to asymmetric stretching vibrations of C34-H36 bond with -99% PED. The experimental frequency correspond to these vibrations is observed at 3014 cm^{-1}.

The theoretically obtained wavenumbers 3123 (for B3LYP), 3151(for CAM-B3LYP) and 3132 (for B3PW91) cm-1 corresponding to C26-H27 vibration corresponds to asymmetric stretching vibrations of C26-H27 bond with PED of -13%. The experimental frequency correspond to these vibrations are not observed.

In TMP, the theoretical frequencies at 1160 (for B3LYP), 1177 (for CAM-B3LYP) and 1163 (for B3PW91) cm^{-1} correspond to C30 -O23 bond vibrations with 64% PED and experimentally the corresponding vibrations are appeared at 1130cm^{-1}. The wavenumbers computed at 1027(for B3LYP), 1061(for CAM-B3LYP) and 1049(forB3PW91) cm^{-1} correspond to stretching mode of C26-O24 vibrations with 77% PED and corresponding experimental frequencies are appeared at 1000 cm^{-1}. These wavenumbers are in good agreement with literature values[39].

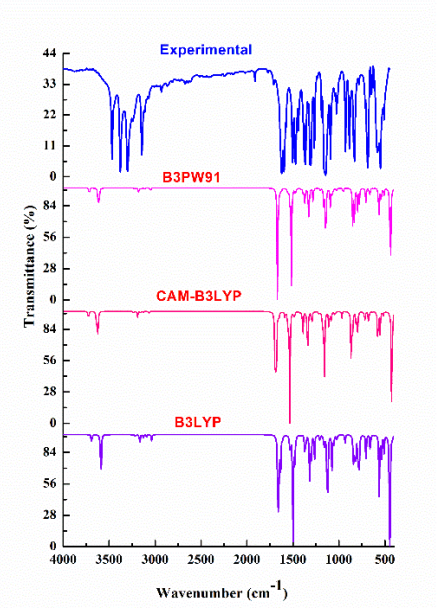

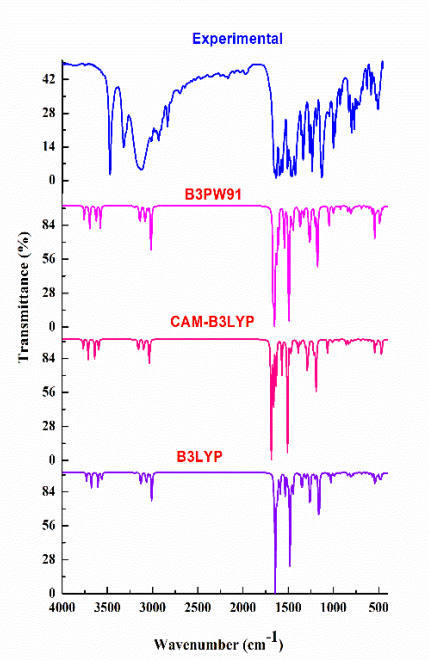

Fig.6(a) Fig. 6(b)

Fig.6. Experimental and Theoretical FT-IR Spectra of (a) SMX and (b) TMP molecules

Table 6(a). Experimental and Theoretical Vibrational assignments of SMX

Modes	**Experimental frequency (cm^{-1})**	**Calculated frequency (cm^{-1})**			**PED(>10%) – for B3LYP**
		B3LYP	CAM-B3LYP	B3PW91	
1	-	3690	3725	3716	υ(N11-H12)(-50)+υ (N11-H13) (50)
2	-	3591	3635	3618	υ(N17-H18)(100)
3	3468	3586	3620	3608	υ(N11-H12)(50)+υ (N11-H13) (50)
4	3245	3260	3283	3273	υ(C20-H21) (99)
5	-	3216	3236	3223	υ(C5-H9) (98)
6	-	3203	3223	3210	υ(C3-H8)(96)
7	-	3167	3191	3178	υ(C6-H10) (96)
8	3142	3165	3189	3176	υ(C2-H7) (94)
9	3112	3128	3158	3149	υ(C25-H27)(82)
10	3073	3092	3129	3113	υ(C25-H26) (-49)
11	2933	3038	3067	3049	υ(C25-H27)(-18)+υ(C25-H26)(-43)+υ(C25-H28)(-40)
12	1710	1663	1696	1668	SCI(H13-N11-H12)(75)
13	-	1654	1682	1666	υ(C20-C22)(53)+υ(N23-C19)(-18)
14	1623	1635	1660	1645	υ(C2-C3)(27)+υ(C6-C5)(10)
15	1598	1612	1651	1627	υ(C5-C4)(-25)+υ(C1-C6)(20)+β(C1-C6-C5)(-15)
16	1575	1537	1587	1556	υ(N23-C19)(51)+υ(N17-C19)(-11)
17	-	1529.	1555	1535	β(H8-C3-C2)(16)+β (H7-C2-C3) (-13)

Modes	**Experimental frequency (cm^{-1})**	**Calculated frequency (cm^{-1})**			**PED(>10%) – for B3LYP**
18	1500	1499	1535	1515	υ(N17-C19)(16)
19	-	1481	1493	1478	υ(H26-C25-H28)(36)
20	1474	1474	1486	1469	β(H28-C25-H27)(38)
21	1440	1463	1481	1467	υ(C2-C3)(-19)
22	-	1416	1426	1407	β(H27-C25-H26)(-30)
23	1365	1368	1392	1386	β(H18-N17-C19)(22)
24	-	1357	1362	1369	υ(C4-C3)(-10)+β(H18-N17-C19)(13)
25	-	1332	1342	1332	υ(C4-C3)(14)
26	1311	1318	1339	1329	υ(N11-C1)(50)
27	1305	1303	1336	1323	υ(S14-O15)(-42)+υ(S14-O16)(30)
28	1266	1266	1294	1280	β(H18-N17-C19)(30)
29	-	1206	1216	1203	β(H10-C6-C1)(-22)+β(H9-C5-C6)(-14)+β(H8-C3-C2)(-14)
30	1187	1160	1177	1164	υ(N17-C19)(12)+υ(C25-C22)(-17)+β(H21-C20-C22)(49)
31	1144	1152	1159	1149	β(H8-C3-C2)(13)+υ(C2-C3)(10)+β(H7-C2-C3)(21)+β(H10-C6-C1)(17)+ β(H9-C5-C6)(11)
32	-	1124	1157	1142	υ(C4-C3)(-12)+υ(C5-C4)(-11)+υ(S14-O15)(-17)+υ(S14-O16)(-25)+υ(S14-C4)(14)
33	1091	1075	1107	1091	υ(C4-C3)(15)+υ(C5-C4)(13)+υ(CS14-O15)(-19)+(S14-O16)(-27)

Modes	Experimental frequency (cm^{-1})	Calculated frequency (cm^{-1})			PED(>10%) – for B3LYP
34	-	1070	1086	1072	υ(C1-C6)(-17)+β(H12-N11-C1)(54)
35	-	1063	1078	1069	β(H27-C25-H26)(13)+β(H28-C25-H27)(-13)+T(H27-C25-C22-C20)(-57)
36	1040	1054	1074	1055	υ(O24-C25)(32)+υ(O24-C22)(32)+υ(N17-C19)(13)+β(C20-C22-O24)(26)
37	1027	1029	1047	1032	υ(C20-C22-C23)+β(H21-C20-C22)(15)+β(C22-O24-N23)(-17)+T(H26-C25-C22-C20)(10)+T(H28-C25-C22-C20)(-11)
38	1015	1020	1034	1020	β(C6-C5-C4)(20)+β(C2-C3-C4)(39)+β(C5-C4-C3)(-21)
39	-	1006	1032	1017	υ(O24-N23)(17)+υ(O27-C22)(-11)+β(C22-O24-N23)(27)+T(H26-C25-C22-C20)(11)+T(H28-C25-C22-C20)(-11)
40	989	975	1002	973	T(H7--C4-C2-C3)(12)+T(H8-C3-C4-S14)(-38)+T(H9-C5-C4-S14)(-28)+T(H10-C6-C1-N11)(-15)
41	928	962	985	958	T(H8-C3-C4-S14)(26)+T(H9-C5-C4-S14)(-30)+T(H10-C6-C1-N11)(-14)
42	886	932	968	952	υ(O24-N23)(49)+β(C20-C22-O24)(14)

Modes	**Experimental frequency (cm^{-1})**	**Calculated frequency (cm^{-1})**			**PED(>10%) – for B3LYP**
43	-	843	865	850	υ(N11-C1)(11)+β(C5-C4-C3)(31)
44	830	832	855	834	T(H7-C2-C3-C4)(-16)+T(H9-C5-C4-S14)(13)+T(H10-C6-C1-N11)(-30)
45	-	818	848	830	υ(N17-C19)(13)+υ(S14-N17)(-28)
46	-	816	836	816	T(H7-C2-C3-C4)(16)+T(H9-C5-C4-S14)(13)+T(H10-C6-C1-N11)(-26)
47	-	790	810	798	OUT(C25-C20-O24-C22)(-12)+T(C22-O24-N23-C19)(10)
48	780	778	794	777	T(H21-C20-C22-C25)(-72)
49	-	731	738	732	T(C1-C6-C5-C4)(-25)+OUT(N11-C6-C2-C1)(-21)
50	714	704	718	706	T(C20-C22-O24-N23)(29)+T(C22-O24-N23-C19)(-33)
51	685	660	676	666	υ(C25-C22)(28)+β(C20-C22-O24)(-30)
52	-	655	674	664	υ(C25-C22)(13)+υ(S14-C4)(-20)
53	644	647	654	644	β(C2-C3-C4)(-18)+β(C6-C5-C4)(36)
54	617	618	633	622	T(C20-C22-O24-N23)(29)+T(C22-O24-N23-C19)(-30)
55	580	561	576	565	β(O15-S14-O17)(-23)+β(N17-S14-C4)(16)

Modes	Experimental frequency (cm^{-1})	Calculated frequency (cm^{-1})			PED(>10%) – for B3LYP
56	547	537	551	540	OUT(O15-N17-O16-N14)(45)
57	508	508	515	509	β(O15-S14-O16)(22)+OUT(N11-C6-C2-C1)(-27)
58	-	447	451	445	T(H12-N11-C1-C6)(-30)+T(H13-N11-C1-C6)(28)
59	-	422	428	438	T(O24-N23-C19-N17)(14)
60	-	418	426	422	T(C2-C3-C4-C5)(-26)

β= Bending, OUT=out of plane bending, SCI- scissoring, υ= Stretching T= Torsion,

Table 6(b). Experimental and Theoretical Vibrational assignments of TMP

Modes	Experimental frequency (cm^{-1})	Calculated frequency (cm^{-1})			PED(>10%) – for B3LYP
		B3LYP	CAM-B3LYP	B3PW91	
1	-	3730	3767	3755	υ(N7-H8)(100)
2	-	3677	3712	3696	υ(N11-H12)(-100)
3	-	3604	3639	3625	U(N7-H8)(100)
4	3470	3563	3597	3575	υ(N11-H12)(99)
5	-	3203	3227	3208	υ(C19-H22)(99)
6	-	3193	3218	3200	υ(C15-H21)(99)
7	-	3134	3162	3147	υ(C34-H35)(91)
8	-	3133	3161	3146	υ(C30-H32)(92)
9	-	3125	3152	3137	υ(C2-H5)(99)

Modes	**Experimental frequency (cm^{-1})**	**Calculated frequency (cm^{-1})**			**PED(>10%) – for B3LYP**
10	3123	3123	3151	3132	υ(C26-H27) (-13)+υ(C26-H29)(87)
11	-	3075	3102	3089	υ(C26-H27)(98)
12	-	3068	3099	3082	υ(C34-H36)(-99)
13	-	3062	3093	3075	υ(C30-H31)(100)
14	-	3039	3076	3055	υ(C14-H38)(99)
15	3014	3011	3040	3018	υ(C26-H27)(85)+υ(C26-H29)(12)
16	-	3008	3036	3017	υ(C14-H38)(95)
17	-	3008	3035	3015	υ(C14-H38)(94)
18	2964	3004	3031	3010	υ(C30-H31)(91)
19	1655	1653	1688	1664	υ(C2-C3)(-19)+SCI1(H13-N11-H12)(53)
20	1634	1640	1668	1649	υ(C2-C3)(-37)+SCI2(H9-N7-H8)(21)
21	-	1624	1663	1640	υ(C15-C16)(45)+β(H21-C15-C20)(18)
22	-	1622	1662	1636	β(H9-N7-H8)(39)+β(H13-N11-H12)(-12)
23	-	1619	1636	1623	υ(C15-C20)+β(C17-C16-C15)(12)
24	1594	1590	1629	1607	υ(N6-C1)(39)+β(N6-C2-C3)(-10)+β(C1-N10-C4)(-13)
25	1565	1533	1570	1545	υ(C15-C16)(17)+υ(O24-C17)(-10)+β(H21-C15-C20)(16)
26	1507	1504	1512	1500	β(H31-C30-H33)(-70)+T(H31-C30-O23-C16)(10)

Modes	Experimental frequency (cm^{-1})	Calculated frequency (cm^{-1})			PED(>10%) – for B3LYP
27		1503	1511	1499	β(H35-C34-H37)+β(H37-C34-H36)(53)+T(H31-C30-O23-C16)(11)
28	-	1500	1511	1495	β(H28-C26-H29)(-68)+T(H27-C26-O24-C17)(-13)
29	-	1493	1507	1494	β(H31-C30-H32)(-70)+T(H31-C30-O23-C16)(-25)
30	-	1492	1506	1493	β(H35-C34-H37)(-37)+β(H36-C34-H35)(38)+T(H35-C34-O25-C18)(23)
31	-	1491	1505	1491	β(H27-C26-H29)+β(H31-C30-H32)(10)+T(H27-C26-O24-C17)(-11)
32	1486	1487	1502	1487	β(H27-C26-H29)(42)+T(H27-C26-O24-C17)(16)
33	-	1483	1501	1486	υ(N11-C4)(11)+β(H31-C30-H32)(17)
34	-	1481	1497	1483	β(H31-C30-H32)(40)+β(H35-C34-H37)(10)+β(H36-C34-H35)(13)+β(H37-C34-H36)(10)
35	-	1480	1494	1478	υ(C2-C3)(20)+β(H5-C2-N6)(11)+β(N10-C1-N6)(16)
36	1459	1466	1480	1461	β(H39-C14-H38)(55)
37	-	1464	1476	1459	β(H27-C26-H28)(76)

Modes	**Experimental frequency (cm^{-1})**	**Calculated frequency (cm^{-1})**			**PED(>10%) – for B3LYP**
38	1445	1446	1467	1447	υ(C15-C16)(16)+β(H22-C19-C20)(26)+β(H31-C30-H32)(15)
39	-	1380	1408	1392	υ(C2-C3)(47)
40	1355	1355	1387	1373	υ(O25-C18)(43)+β(H38-C14-C20)(11)
41	-	1346	1361	1364	υ(C19-C20)(42)
42	1335	1340	1351	1341	υ(N11-C4)(10)+β(H5-C2-N6)(53)
43	-	1309	1317	1328	υ(N6-C2)(12)+υ(C19-C20)(10)+T(H38-C14-C20-C15)(17)
44	-	1302	1306	1311	υ(N6-C2)(-51)+β(H8-N7-C1)(-11)
45	1264	1262	1289	1268	β(H22-C19-C20)(54)
46	-	1257	1278	1258	υ(O24-C17)(40)
47	1236	1228	1248	1234	υ(C3-C14)(-29)+T(H39-C14-C20-C15)(19)
48	-	1209	1220	1207	β(H31-C30-H33)(-10)+T(H31-C30-O23-C16)(60)
49	-	1204	1217	1205	T(H27-C26-O24-C17)(48)
50	-	1202	1215	1201	β(H38-C14-C20)(24)+T(H27-C26-O24-C17)(26)
51	-	1201	1212	1201	β(H38-C14-C20)+T(H27-C26-O24-C17)(30)
52	1189	1171	1194	1178	υ(N6-C2)(-22)+υ(N11-C4)(-10)+β(H8-N7-C1)(42)
53	-	1168	1188	1176	β(H31-C30-H32)(21)+T(H31-C30-O23-

Modes	Experimental frequency (cm^{-1})	Calculated frequency (cm^{-1})			PED(>10%) – for B3LYP
					C16)(61)+T(H35-C34-O25-C18)(-12)
54	-	1167	1181	1170	β(H36-C34-H35)+T(H35-C34-O25-C18)(-59)
55	-	1166	1180	1167	υ(C15-C20)(20)+υ(C14-C20)(-13)+β(H21-C15-C20)(30)
56	-	1164	1180	1166	β(H27-C26-H29)(23)+T(H27-C26-O24-C17)(67)
57	1130	1160	1177	1163	υ(O23-C30)(64)
58	-	1069	1103	1088	υ(O23-C30)(66)
59	1058	1056	1066	1056	υ(N6-C1)(21)+β(H8-N7-C1)(61)
60	1000	1027	1061	1049	υ(O24-C26)(77)
61		996	1015	1001	υ(C2-C3)(29)+β(C1-N6-C2)(-13)+β(C1-N10-C4)(-10)
62	986	983	1005	992	υ(C14-C20)(21)+T(H5-C2-N6-C1)(-20)
63	969	971	994	972	T(H5-C2-N6-C1)(52)
64	-	946	969	957	υ(O23-C16)(-40)+T(H38-C14-C20-C15)(-10)
65	927	920	939	922	υ(O23-C16)(-27)+T(H38-C14-C20-C15)(16)
66	908	845	868	841	T(H22-C19-C20-C14)(-65)
67	830	837	859	834	T(H21-C15-C20-C14)(56)
68	-	811	832	811	T(H21-C15-C20-C14)(12)+T(C1-N6-C2-C3)(-51)

Modes	**Experimental frequency (cm^{-1})**	**Calculated frequency (cm^{-1})**			**PED(>10%) – for B3LYP**
69	805	806	819	808	υ(C3-C14)(11)+β(N6-C2-C3)(12)
70	798	798	817	801	υ(C3-C14)(12)+β(C15-C20-C19)(10)+T(C17-C16-C15-C20)(-15)
71	782	777	793	782	υ(N6-C1)(17)+β(C1-N6-C2)(14)+β(N6-C2-C3)(-11)+β(N10-C1-N6)(13)
72	768	762	779	764	T(C17-C16-C15-C20)(17)
73	741	736	753	739	OUT(N7-N6-N10-C1)(68)
74	677	686	698	688	υ(C5-C20)(-11)
75	630	643	652	643	β(C16-C15-C20)(39)
76	-	617	633	619	β(C1-N10-C4)(18)
77	597	608	616	608	OUT(O23-C15-C16)(11)
78	584	584	594	584	β(C1-N10-C4)(-11)
79	566	569	577	570	T(C15-C20-C19-C18)(12)+OUT(C14-C15-C19-C20)(10)
80		540	543	543	β(N10-C4-N11)(-11)+T(H12-N11-C4-C3)(58)
81	529	535	542	535	υ(O23-C16)(10)+β(C16-C15-C20)(13)+β(C18-C17-O24)(-39)
82	-	521	527	521	β(N10-C4-N11)(17)+T(H8-N7-C1-N6)(-16)
83	506	508	517	509	β(N10-C4-N11)(-12)+T(H8-N7-C1-N6)(31)
84	-	487	493	491	T(H9-N7-C1-N6)(-65)

Modes	Experimental frequency (cm^{-1})	Calculated frequency (cm^{-1})			PED(>10%) – for B3LYP
85	-	475	468	476	β(N10-C4-N11)(14)+T(H8-N7-C1-N6)(33)+T(N9-N7-C1-N6)(14)+T(C1-N6-C2-C3)(12)
86	454	454	462	454	T(H12-N11-C3-C4)(-12)+T(H5-C2-N6-C1)(13)+T(C1-N6-C2-C3)(51)
87	-	421	430	422	β(C17-O24-C26)(18)+T(H8-N7-C1-N6)(-16)

β= Bending, OUT=out of plane bending, SCI- scissoring,υ= Stretching T= Torsion,

4. Conclusion

The theoritically obtained bond length and bond angles of SMX and TMP from B3LYP and B3PW91 theories at 6-311++G(d,p) basis set are in good agreement with literature XRD data. The FMO study demonstrates that TMP is more chemically stable than SMX. MEP map analysis revealed that oxygen atoms present in sulfamethoxazole group of SMX and methoxy group of TMP are more electron-rich and hence they are best sites for electrophilic attack. Mulliken atomic charge study shows that the C3 and C20 atoms exhibit more positive charge in TMP, whereas C1, C19 and C22 atoms exhibits more positive charge in SMX. The NLO study of SMX and TMP reveals that these molecules are potential candidates for NLO applications. NBO analysis reflects that, the SMX shows more intensive intramolecular interaction between LP(2) (O24) and π* (C20-C22), whereas TMP shows the intensive intramolecular interaction between σ (C14-H39) and σ (C34-H37). The good agreement of experimental vibrational frequencies of SMX and TMP with theoretically obtained frequencies signifies the importance of quantum chemical calculations.

Acknowledgements:
The author Vibha thanks Govt. of Karnataka for awarding monthly scholarship under Backward Class Welfare Department to pursue Ph.D. at Dept. of Physics, Vijayanagara Sri Krishnadevaraya University, Ballari, Karnataka, India.

References:

[1] A. Ovung and J. Bhattacharyya, "Sulfonamide drugs: structure, antibacterial property, toxicity, and biophysical interactions," *Biophysical Reviews*, vol. 13, no. 2. Springer, pp. 259–272, Mar. 2021. doi: 10.1007/s12551-021-00795-9.

[2] S. P. Vijayachamundeshwari, E. J. J. Samuel, and N. Sundaraganesan, "Molecular structure , vibrational spectra , NMR and UV spectral analysis of," *Spectrochim. ACTA PART A Mol. Biomol. Spectrosc.*, 2013, doi: 10.1016/j.saa.2013.07.063.

[3] D. Das *et al.*, "Spectrochimica Acta Part A : Molecular and Biomolecular Spectroscopy The crystal structure of sulfamethoxazole , interaction with DNA , DFT calculation , and molecular docking studies," *Spectrochim. ACTA PART A Mol. Biomol. Spectrosc.*, vol. 137, pp. 560–568, 2015, doi: 10.1016/j.saa.2014.08.034.

[4] M. C. Almandoz, M. I. Sancho, and S. E. Blanco, "Spectrochimica Acta Part A : Molecular and Biomolecular Spectroscopy Spectroscopic and DFT study of solvent effects on the electronic absorption spectra of sulfamethoxazole in neat and binary solvent mixtures," *Spectrochim. ACTA PART A Mol. Biomol. Spectrosc.*, vol. 118, pp. 112–119, 2014, doi: 10.1016/j.saa.2013.08.060.

[5] A. Ungurean, N. Leopold, L. David, and V. Chis, "Spectrochimica Acta Part A : Molecular and Biomolecular Spectroscopy Vibrational spectroscopic and DFT study of trimethoprim," vol. 102, pp. 52–58, 2013, doi: 10.1016/j.saa.2012.10.026.

[6] T. Van Mourik, M. Bühl, and M. P. Gaigeot, "Density functional theory across chemistry, physics and biology," *Philos. Trans. R. Soc. A Math. Phys. Eng. Sci.*, vol. 372, no. 2011, 2014, doi: 10.1098/rsta.2012.0488.

[7] M. Takasuka and H. Nakai, "IR and Raman spectral and X-ray structural studies of polymorphic forms of sulfamethoxazole," *Vib. Spectrosc.*, vol. 25, no. 2, pp. 197–204, 2001, doi: 10.1016/S0924-2031(01)00089-3.

[8] L. A. J. Rodríguez-Blanco, R. Ocampo-Pérez, C. F. A. Gómez-Durán, J. P. Mojica-Sánchez, and R. S. Razo-Hernández, "Removal of sulfamethoxazole, sulfadiazine, and sulfamethazine by UV radiation and HO• and SO4•− radicals using a response surface model and DFT calculations," *Environ. Sci. Pollut. Res.*, vol. 27, no. 33, pp. 41609–41622, Nov. 2020, doi: 10.1007/S11356-020-10071-0.

[9] K. R. Genik Ea, Biryukova Mm, Zolotareva Nv, Kemelbaeva Dr, "Structure, Vibration Frequencies And Thermodynamic Properties of Trimethoprim: The Quantumchemical Studies,"," p. P 308, 2016.

[10] N. A. Khudhair, M. M. Kadhim, and A. A. Khadom, "Effect of Trimethoprim Drug Dose on Corrosion Behavior of Stainless Steel in Simulated Human Body Environment: Experimental and Theoretical Investigations," *J. Bio- Tribo-Corrosion*, vol. 7, no. 3, pp. 1–15, 2021, doi: 10.1007/s40735-021-00559-8.

[11] FilizÖztürk, "Structural characterization (XRD, FTIR) and magnetic studies of Cd(II)-Sulfamethoxazole-2,2′-bipyridine: DFT and Hirshfeld Surface Analysis,"," *J. Mol. Struct.*, vol. 1271.

[12] M. Z. Ahmed and U. Habib, "DFT studies of temperature effect on coordination chemistry of Cu(II)-trimethoprim complexes," *J. Coord. Chem.*, vol. 71, no. 8, pp. 1102–1113, 2018, doi: 10.1080/00958972.2018.1447667.

[13] K. D. K. R. Biryukova Mm , Genik Ea , Zolotareva Nv, "The Quantumchemical Studies Of Structure And Properties Of Sulfamethoxazole In Composition Of The Drug 'Biseptol," p. 92, 2016.

[14] R. D. Denningham II, T. A. Keith, and J. Millan, "Gauss View, Version 4.1.2," *Semichem Inc, Shawnee Mission KS,* 2003.

[15] J. R. M.J. Frisch, G.W. Trucks, H.B. Schlegel, G.E. Scuseria, M.A. Robb, J.R. Cheeseman, G. Scalmani, V. Barone, B. Mennucci, G.A. Petersson, H. Nakatsuji, M. Caricato, X. Li, H.P. Hratchian, A.F. Izmaylov, J. Bloino, G. Zheng, J.L. Sonnenberg, M.Hada, M. Ehara, K. Toyota, R. Fukuda, J. Hasegawa, M. Ishida, T. Nakajima, Y. HondaO. Kitao, H. Nakai, T. Vreven, J.A. Montgomery, J.E. Peralta, F. Ogliaro, M. BearparkJ.J. Heyd, E. Brothers, K.N. Kudin, V.N. Staroverov, R. Kobayashi, J. Normand, K.Raghavachari, A. Rendell, J.C. Burant, S.S. Iyengar, J. Tomasi, M. Cossi, N. Rega, J.M.Millam, M. Klene, J.E. Knox, J.B. Cross, V. Bakken, C. damo, J. Jaramillo, R.Gomperts, R.E. Stratmann, O. Yazyev, A.J. Austin, R. Cammi, C.Pomelli, J.W. chterskiR.L. Martin, K. Morokuma, V.G. Zakrzewski, G.A. Voth, P. Salvador, J.J. DannenbergS. Dapprich, A.D. Daniels, Farkas, J.B. Foresman, J.V. Ortiz, J. Cioslowski, D.J. Fox "Gaussian 09, Revision B.01," *Gaussian, Inc*.2010.

[16] P. V. R. S. Timothy Clark, Jayaraman Chandrasekhar, Günther W. Spitznagel, "Efficient diffuse function-augmented basis sets for anion calculations. III.† The 3-21+G basis set for first-row elements, Li–F," 1983.

[17] M. H. Jamróz, "Vibrational energy distribution analysis (VEDA): Scopes and limitations," *Spectrochim. Acta - Part A Mol. Biomol. Spectrosc.*, vol. 114, pp. 220–230, 2013, doi: 10.1016/J.SAA.2013.05.096.

[18] E. D. Glendening, C. R. Landis, and F. Weinhold, "NBO 6.0: Natural bond orbital analysis program," *J. Comput. Chem.*, vol. 34, no. 16, pp. 1429–1437, 2013, doi: 10.1002/jcc.23266.

[19] L. Maury, J. Rambaud, B. Pauvert, Y. Lasserre, G. Berge, and M. Audran, "Étude Physico-Chimique, Spectres De Vibration Et Structure Du Sulfaméthoxazole," *Can. J. Chem.*, vol. 63, no. 11, pp. 3012–3018, 1985, doi: 10.1139/v85-500.

[20] T. Yanai, D. P. Tew, and N. C. Handy, "A new hybrid exchange-correlation functional using the Coulomb-

attenuating method (CAM-B3LYP)," *Chem. Phys. Lett.*, vol. 393, no. 1–3, pp. 51–57, 2004, doi: 10.1016/j.cplett.2004.06.011.

[21] J. Prashanth, G. Ramesh, J. L. Naik, J. Kishan, and B. V. Reddy, "ScienceDirect Molecular geometry , NBO analysis , Hyperpolarizability and HOMO-LUMO energies of 2-azido-1-phenylethanone using Quantum chemical calculations," *Mater. Today Proc.*, vol. 3, no. 10, pp. 3761–3769, 2016, doi: 10.1016/j.matpr.2016.11.025.

[22] L. G. Zhuo, W. Liao, and Z. X. Yu, "A Frontier Molecular Orbital Theory Approach to Understanding the Mayr Equation and to Quantifying Nucleophilicity and Electrophilicity by Using HOMO and LUMO Energies," *Asian J. Org. Chem.*, vol. 1, no. 4, pp. 336–345, 2012, doi: 10.1002/ajoc.201200103.

[23] A. Chandran *et al.*, "Spectrochimica Acta Part A : Molecular and Biomolecular Spectroscopy FT-IR , FT-Raman and computational study of (E) - N -carbamimidoyl-4- ((4-methoxybenzylidene) amino) benzenesulfonamide," *Spectrochim. Acta Part A Mol. Biomol. Spectrosc.*, vol. 92, pp. 84–90, 2012, doi: 10.1016/j.saa.2012.02.030.

[24] J. Fang and J. Li, "Quantum chemistry study on the relationship between molecular structure and corrosion inhibition efficiency of amides," vol. 593, pp. 179–185, 2002.

[25] E. S. Marinho and M. M. Marinho, "A DFT study of synthetic drug topiroxostat: MEP, HOMO, LUMO," vol. 7, no. 8, pp. 1264–1270, 2016.

[26] E. B. Masoome Sheikhia,* and and H. Laric, "Theoretical investigations on molecular structure, NBO, HOMO-LUMO and MEP analysis of two crystal structures of N -(2 -benzoyl-phenyl) oxalyl: A DFT study Masoome Sheikhi," *J. Phys. Theor. Chem.*, vol. 13, 2016.

[27] S. S. Khemalapure, S. M. Hiremath, C. S. Hiremath, V. S. Katti, and M. M. Basanagouda, "Investigations of structural, vibrational and electronic properties on 5-(6-methyl-benzofuran-3-ylmethyl)-3H-[1,3,4]oxadiazole-2-thione:

Experimental and computational approach," *Chem. Data Collect.*, vol. 28, 2020, doi: 10.1016/j.cdc.2020.100410.

[28] E. A. Bisong *et al.*, "Heliyon Vibrational , electronic , spectroscopic properties , and NBO analysis of xylene : DFT study," *Heliyon*, vol. 6, no. December, p. e05783, 2020, doi: 10.1016/j.heliyon.2020.e05783.

[29] M. Kurt, P. C. Babu, N. Sundaraganesan, M. Cinar, and M. Karabacak, "Molecular structure, vibrational, UV and NBO analysis of 4-chloro-7-nitrobenzofurazan by DFT calculations," *Spectrochim. Acta - Part A Mol. Biomol. Spectrosc.*, vol. 79, no. 5, pp. 1162–1170, 2011, doi: 10.1016/j.saa.2011.04.037.

[30] F. W. Asker and Z. Z. Mahamad, "Synthesis and characterization of some sulfonamide dervatives," vol. 13, no. 2, pp. 169–177, 2017.

[31] D. Ramarajan, K. Tamilarasan, and S. Sudha, "Synthesis , crystal structure analysis and DFT studies of," *J. Mol. Struct.*, vol. 1139, pp. 282–293, 2017, doi: 10.1016/j.molstruc.2017.03.045.

[32] S. P. Vijayachamundeeswari and H. Umamahesvari, "Quantum Chemical and spectroscopic (FT-IR , FT Raman , NMR and UV) analysis of Antibiotic drug Sulfachloropyridazine," no. 4, 2019.

[33] E. Başar, E. Tunca, M. Bülbül, M. Kaya, and E. Ba, "Synthesis of novel sulfonamides under mild conditions with effective inhibitory activity against the carbonic anhydrase isoforms I and II Synthesis of novel sulfonamides under mild conditions with effective inhibitory activity against the carbonic anhydra," vol. 6366, 2016, doi: 10.3109/14756366.2015.1134524.

[34] I. Gulaczyk *et al.*, "The NH 2 scissors band of methylamine To cite this version : HAL Id : hal-02344590," 2019.

[35] N. G. P. Roeges, "Roeges N.G.P., A Guide to the Complete Interpretation of the Infrared Spectra of Organic Structures. Wiley, NY, 1994.," 1994.

[36] P. Govindasamy and S. Gunasekaran, "Quantum mechanical calculations and spectroscopic (FT-IR , FT-Raman and UV)

investigations , molecular orbital , NLO , NBO , NLMO and MESP," *J. Mol. Struct.*, vol. 1081, pp. 96–109, 2015, doi: 10.1016/j.molstruc.2014.10.011.

[37] J. Prashanth, G. Ramesh, J. L. Naik, J. K. Ojha, B. V. Reddy, and G. R. Rao, "Molecular Structure, Vibrational Analysis and First Order Hyperpolarizability of 4-Methyl-3-Nitrobenzoic Acid Using Density Functional Theory," *Opt. Photonics J.*, vol. 05, no. 03, pp. 91–107, 2015, doi: 10.4236/opj.2015.53008.

[38] M. K. Subramanian, P. M. Anbarasan, and S. Manimegalai, "Spectrochimica Acta Part A : Molecular and Biomolecular Spectroscopy DFT simulations and vibrational analysis of FT-IR and FT-Raman spectra of," vol. 73, pp. 642–649, 2009, doi: 10.1016/j.saa.2009.03.006.

[39] T. Chithambarathanu, K. Vanaja, and J. Daisymagdaline, "Quantum Chemical Calculations on Vibrational and Electronic Structure Of3- (4-Methoxybenzoyl) Prop ionic Acid," vol. 11, no. 3, pp. 42–53, 2018, doi: 10.9790/5736-1103014253.